Advances in Nano Research, *Vol. 14, No. 5 (2023) 463-474*
https://doi.org/10.12989/anr.2023.14.5.463

Propagating and evanescent waves in a functionally graded nanoplate based on nonlocal theory

Cancan Liu, Jiangong Yu*, Bo Zhang, Xiaoming Zhang and Xianhui Wang

School of Mechanical and Power Engineering, Henan Polytechnic University, Jiaozuo 454003, P.R. China

(*Received February 5, 2022, Revised April 1, 2022, Accepted July 8, 2022*)

Abstract. The purpose of this paper is to present the analysis of propagating and evanescent waves in functionally graded (FG) nanoplates with the consideration of nonlocal effect. The analytical integration nonlocal stress expansion Legendre polynomial method is proposed to obtain complete dispersion curves in the complex domain. Unlike the traditional Legendre polynomial method that expanded the displacement, the presented polynomial method avoids employing the relationship between local stress and nonlocal stress to construct boundary conditions. In addition, the analytical expressions of numerical integrations are presented to improve the computational efficiency. The nonlocal effect, inhomogeneity of medium and their interactions on wave propagation are studied. It is found that the nonlocal effect and inhomogeneity of medium reduce the frequency bandwidth of complex evanescent Lamb waves, and make complex evanescent Lamb waves have a higher phase velocity at low attenuation. The occurrence of intersections of propagating Lamb wave in the nonlocal homogeneous plate needs to satisfy a smaller Poisson's ratio condition than that in the classical elastic theory. In addition, the inhomogeneity of medium enhances the nonlocal effect. The conclusions obtained can be applied to the design and dynamic response evaluation of composite nanostructures.

Keywords: evanescent wave; functionally graded materials; legendre orthogonal polynomial; nanostructures; nonlocal theory; propagating wave

1. Introduction

As a novel type of composites, functionally graded materials (FGMs) are indispensable candidates for mechanical designs due to their improved corrosion resistance, toughness and lower stress concentration (Ebrahimi *et al*. 2018a). FG nanoscale structures have great potential to improve the overall operation of many nanoelectromechanical systems (NEMS) due to tunable material properties (Ghayesh and Farajpour 2019). Mechanical Properties Characterization of nanomaterials is essential for structural design and application. Due to the well-known fact that the mechanics of nanostructures are highly size-dependent, the classical continuum mechanics theory is not available. Moreover, experimental studies on nanomaterials are inherently complex and challenging, and molecular dynamics is computationally expensive and not even applicable to systems with large numbers of molecules. Consequently, the non-classical continuum mechanic models, such as nonlocal theory (Eringen 1983), modified couple stress theory (Yang *et al*. 2002), surface effect theory (Lu *et al*. 2006), strain gradient theory (Mindlin 1965) and combined non-classical theory (Amiri *et al*. 2019, Ardalani *et al*. 2021), are identified to be suitable alternatives to estimate the size dependence of mechanical characteristic. The nonlocal theory recommend by Eringen shows that the stress state of a particle is related to both the strain of the particle itself and the strain of other surrounding particles. Recently, besides nonlocal models of typical structures, mechanical models of FG nonlocal structures have also attracted the attention of many scientific researches. Based on Eringen's works, many works on free vibration (Ahmadi 2021, Zhang *et al*. 2019, Hadji and Avcar 2021, Ehyaei 2016), buckling (Nejad *et al*. 2016, Luat *et al*. 2021) and bending (Chaht *et al*. 2015, Tran *et al*. 2021) of various FG nanostructures have been reported.

The importance of wave propagation in nanostructures has been demonstrated in various applications such as mechanical property characterization (Hernandez *et al*. 2002), biomechanical studies (Elayan *et al*. 2017) and the design of acoustically driven nanogenerators (Cha *et al*. 2010). For these reasons, propagating waves in FG nanostructures have been extensively studied. Arefi (2016) investigated wave propagation in nano-rod by accounting nonlocal elasticity and surface effect. Ebrahimi and Haghi (2018b) presented elastic wave dispersion modelling within rotating FG nanobeams in thermal environment. Zhang *et al*. (2015) studied the flexural wave propagation of piezo-electric FG nanobeam with thermal effects. He *et al*. (2021) investigated wave propagation of FG cylindrical nanoshell by a semi-analytical method. In addition to the study of free nanostructures, the analysis of nanostructures naturally includes a substrate. For an example, Ebrahimi *et al*. (2018a) examined the wave propagation behavior of size-dependent FG nanoplates resting on Winkler-Pasternak foundation subjected to thermal loading.

Wave propagation techniques have been discussed to have great potential in nanostructure defect detection

*Corresponding author, Professor,
E-mail: jiangongyu@126.com

ISSN: 2287-237X (Print), 2287-2388 (Online)

(Chong 2008). However, since propagating waves are susceptible to environmental and operational changes, defect detection methods based on propagating waves may generate false positives. Fortunately, complex evanescent waves are of great value in describing defect phenomena due to their unique properties. Lyon (1955) calculated the pure imaginary roots of the long-term equation, which correspond to infinite wavelength modes starting from the cutoff frequency of the Lamb mode. Subsequently, the presence of complex roots of the Rayleigh–Lamb equation was demonstrated and a complete picture of the topology of real, imaginary, and complex wave number dispersion was presented (Mindlin 1958, Mindlin and Medick 1959). Yan and Yuan (2015) discussed the potential implantation of evanescent waves in nondestructive testing. The screening of complex waves with high speed and low attenuation is of great significance for improving the resolution and energy conversion efficiency of devices. Therefore, many papers have focused on the complex waves in various macro structures (Quintanilla *et al*. 2016, Yan and Yuan 2018, Zhu *et al*. 2018, Zhang *et al*. 2018). Recently, efforts have been made towards complex wave dispersion analysis of nano-scale structures. Kaviani and Mirdamadi (2013) derived complex wave dispersion relations and corresponding characteristic equations in carbon nano-tube (CNT) conveying fluid using the strain/inertial gradient theory. They observed Knudsen number could impress complex wave frequencies at both lower and higher ranges of wave numbers, while small-size had impression at higher ranges. Jornet and Akyildiz (2013) proposed a novel nanoantenna based on graphene nanoribbons (GNRs) and derived the dynamic complex wave vector of Surface Plasmon Polariton (SPP) waves in GNRs. Oveissi and Ghassemi (2018) solved the complex-valued wave dispersion relations of the stationary and the axially moving CNTs based the nonlocal elasticity theory. Gopalakrishnan and Narendar (2013) presented complex wavenumber dispersion in monolayer graphene sheets based the nonlocal elasticity theory. Liu *et al*. (2022) discussed the effects of size dependence, piezoelectricity and their interactions on propagative and evanescent waves based the nonlocal elasticity theory. However, although the propagating waves in nanostructures have received extensive attention, the research on complex waves in nanostructures, especially in functionally graded nanostructures, is still very limited. This prompted the authors to investigate complete waves in functionally graded nanostructures.

In recent years, several efficient computational methods, such as Cauchy formalism approach (Kuznetsov 2019, 2021), power series method (Cao *et al*. 2019) and Legendre polynomial method (Liu *et al*. 2021), have been developed to solve wave propagation in functionally graded media. In fact, Legendre polynomial method has been widely utilized to solve guided waves in layered structures (Othmani *et al*. 2020), functionally graded structures (Yang *et al*. 2022) and quasicrystal structures (Zhang *et al*. 2022). The above literatures all extend the mechanical displacement to Legendre polynomial series. However, it is hard to connect local and nonlocal stresses and satisfy nonlocal stress boundary conditions with the displacement expansion

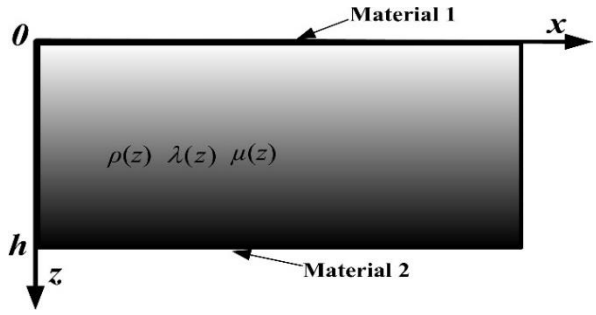

Fig. 1 The schematic diagram of FGM plate with nanoscale

Legendre polynomial method. Recently, Liu *et al*. 2022 developed a nonlocal stress expansion Legendre polynomial method (NSLPM) to study complete guided waves in piezoelectric nanoplates. The complex operations and calculations performed by the displacement expansion method in order to connect local and nonlocal stresses and satisfy the boundary conditions are avoided. However, the NSLPM used in (Liu *et al.* 2022) involves a large number of numerical integration steps, and it is often computationally costly to compute these integrals. To overcome this shortcoming, the analytical integration nonlocal stress expansion Legendre polynomial method (AINSLPM) is proposed to obtain the complete dispersion curves in functionally graded nano-structure. The analytical integration instead of numerical integration is utilized to improve the computational efficiency. This algorithm provides a suitable computational scheme for solving complete waves in nonlocal FGM structure.

2. Nonlocal FGM model

Fig. 1 shows the schematic diagram of a nonlocal FGM plate. The FGM plate is assumed to have thickness h and composed of two isotropic materials. Using the Voigt-type model (Golub *et al*. 2012), the power-law distribution can be expressed as:

$$\lambda(z) = \lambda_2 + (\lambda_1 - \lambda_2)\,(z/h)^n,\ \mu(z) = \mu_2 + (\mu_1 - \mu_2)\,(z/h)^n,\ \rho(z) = \rho_2 + (\rho_1 - \rho_2)\,(z/h)^n \tag{1}$$

where the Lame constants and density are denoted by λ, μ and ρ, respectively. The subscripts 1 and 2 designate the properties of two materials, respectively. The parameter "n" represents the power function parameter.

The nonlocal theory indicates that the stress at a point x depends on the strain at x and all other points x'. The fundamental equations for the nonlocal theory without external forces are given by (Eringen 1983):

$$\sigma_{kl,l} = \rho\ \ddot{u}_k \tag{2}$$

$$\sigma_{kl}(x) = \int_V \alpha(|x' - x|, \tau)\ \sigma_{kl}^c(x')\ dV(x') \tag{3}$$

$$\sigma_{kl}^c(x') = \lambda \varepsilon_{rr}(x')\delta_{kl} + 2\mu\varepsilon_{kl}(x') \tag{4}$$

$$\varepsilon_{kl}(x') = \frac{1}{2}\left(\frac{\partial u_k(x')}{\partial x'_l} + \frac{\partial u_l(x')}{\partial x'_k}\right) \tag{5}$$

Eq. (2) is the equilibrium equations, where σ_{kl}, u_k and ρ are, respectively, the nonlocal stress, displacement and mass density. Eq. (3) shows the relationship between classical stress σ_{kl}^c and nonlocal stress σ_{kl}. Eqs. (4) and (5) indicate the classical constitutive equations and strain-displacement relationships, with λ and μ being Lame constants. The nonlocal modulus $\alpha(|x'-x|,\tau)$ is related to the Euclidean distance $|x'-x|$ and the constant $\tau = e_0 a/L$; where e_0 is an experimentally determined material constant, and L and a are the external and internal characteristics length, respectively. Making certain assumptions, the differential equation form of a nonlocal theory is given by (Eringen 1983):

$$(1 - l^2\nabla^2)\sigma_{kl} = \sigma_{kl}^c \tag{6}$$

where ∇^2 is the Laplacian operator, and $l = e_0 a$ is the nonlocal parameter.

3. Governing equation

3.1 Lamb waves

First, for a plane strain problem (x-z), where the stress and displacement fields are constant in the y direction. According to Eq. (2), the governing equations are:

$$\frac{\partial \sigma_{xx}}{\partial x} + \frac{\partial \sigma_{zx}}{\partial z} = \rho(z)\frac{\partial^2 u_x}{\partial t^2} \tag{7}$$

$$\frac{\partial \sigma_{xz}}{\partial x} + \frac{\partial \sigma_{zz}}{\partial z} = \rho(z)\frac{\partial^2 u_z}{\partial t^2} \tag{8}$$

On the basis of Eqs. (4)-(6), the constitutive relations of FGM plate can be expressed as:

$$\sigma_{xx} - l^2\left(\frac{\partial^2 \sigma_{xx}}{\partial x^2} + \frac{\partial^2 \sigma_{xx}}{\partial z^2}\right) = [\lambda(z) + 2\mu(z)]\frac{\partial u_x}{\partial x} + \lambda(z)\frac{\partial u_z}{\partial z} \tag{9}$$

$$\sigma_{zz} - l^2\left(\frac{\partial^2 \sigma_{zz}}{\partial x^2} + \frac{\partial^2 \sigma_{zz}}{\partial z^2}\right) = \lambda(z)\frac{\partial u_x}{\partial x} + [\lambda(z) + 2\mu(z)]\frac{\partial u_z}{\partial z} \tag{10}$$

$$\sigma_{zx} - l^2\left(\frac{\partial^2 \sigma_{zx}}{\partial x^2} + \frac{\partial^2 \sigma_{zx}}{\partial z^2}\right) = \mu(z)\left(\frac{\partial u_x}{\partial z} + \frac{\partial u_z}{\partial x}\right) \tag{11}$$

Substituting Eqs. (7)-(8) into Eqs. (9)-(11):

$$\begin{aligned}&[\lambda(z) + 2\mu(z)]\left[\frac{1}{\rho(z)}\frac{\partial^2 \sigma_{xx}}{\partial x^2} + \frac{1}{\rho(z)}\frac{\partial^2 \sigma_{zx}}{\partial z \partial x}\right] \\ &+\lambda(z)\frac{\partial}{\partial z}\left[\frac{1}{\rho(z)}\frac{\partial \sigma_{zx}}{\partial x} + \frac{1}{\rho(z)}\frac{\partial \sigma_{zz}}{\partial z}\right] \\ &-\frac{\partial^2}{\partial t^2}\left[\sigma_{xx} - l^2\left(\frac{\partial^2 \sigma_{xx}}{\partial x^2} + \frac{\partial^2 \sigma_{xx}}{\partial z^2}\right)\right] = 0,\end{aligned} \tag{12}$$

$$\begin{aligned}&\lambda(z)\left[\frac{1}{\rho(z)}\frac{\partial^2 \sigma_{xx}}{\partial x^2} + \frac{1}{\rho(z)}\frac{\partial^2 \sigma_{zx}}{\partial z \partial x}\right] + [\lambda(z) \\ &+2\mu(z)]\frac{\partial}{\partial z}\left[\frac{1}{\rho(z)}\frac{\partial \sigma_{zx}}{\partial x} + \frac{1}{\rho(z)}\frac{\partial \sigma_{zz}}{\partial z}\right] \\ &-\frac{\partial^2}{\partial t^2}\left[\sigma_{zz} - l^2\left(\frac{\partial^2 \sigma_{zz}}{\partial x^2} + \frac{\partial^2 \sigma_{zz}}{\partial z^2}\right)\right] = 0,\end{aligned} \tag{13}$$

$$\begin{aligned}&\mu(z)\left[\frac{1}{\rho(z)}\frac{\partial^2 \sigma_{xz}}{\partial x^2} + \frac{1}{\rho(z)}\frac{\partial^2 \sigma_{zz}}{\partial z \partial x}\right] + \mu(z)\frac{\partial}{\partial z}\left[\frac{1}{\rho(z)}\frac{\partial \sigma_{xx}}{\partial x}\right. \\ &\left.+\frac{1}{\rho(z)}\frac{\partial \sigma_{zx}}{\partial z}\right] - \frac{\partial^2}{\partial t^2}\left[\sigma_{zx} - l^2\left(\frac{\partial^2 \sigma_{zx}}{\partial x^2} + \frac{\partial^2 \sigma_{zx}}{\partial z^2}\right)\right] = 0.\end{aligned} \tag{14}$$

To satisfy the boundary conditions ($\sigma_{zz} = \sigma_{zx} = 0$, at z = 0 and z = h), the nonlocal stress components of free harmonic stress waves can be shown as:

$$\sigma_{xx} = U\ \ (z)\, e^{i(kx-\omega t)} \tag{15}$$

$$\sigma_{zz} = z(z-h)V\ \ (z)\, e^{i(kx-\omega t)} \tag{16}$$

$$\sigma_{zx} = z(z-h)W\ \ (z)\, e^{i(kx-\omega t)} \tag{17}$$

where k and ω are the wavenumber and angular frequency, respectively.

Expanding U (z), V (z) and W (z) into Legendre orthogonal polynomial series:

$$\begin{aligned}&U(z) = \sum_{m=0}^{\infty} p_m^1\, Q_m(z),\ V(z) = \sum_{m=0}^{\infty} p_m^2\, Q_m(z), \\ &W(z) = \sum_{m=0}^{\infty} p_m^3\, Q_m(z)\end{aligned} \tag{18}$$

$$\sigma_{zz} = z(z-h)V\ \ (z)\, e^{i(kx-\omega t)} \tag{19}$$

where $L_m(\overline{z})$ represents the m-th Legendre orthogonal polynomial series. Unknown polynomial expansion coefficients are represented by $p_m^i (i = 1,2,3)$. Mapping the integration interval from [0, h] to [-1, 1] by defining $\overline{z} = \frac{2z-h}{h}$. When the effects of higher-order term of polynomial series are negligible, m can be taken as the end order value M.

Substituting Eqs. (15)-(19) into Eqs. (12)-(14), multiplying by $Q_j(z)$ (j = 0…M), and integrating on the interval [0, h], the following matrix equations can be obtained:

$$k^2 A\ p + k\ B\ p + C\ p\ = 0 \tag{20}$$

where

$$\begin{aligned}A &= \begin{bmatrix} A_{11}^{j,m} & 0 & 0 \\ A_{21}^{j,m} & 0 & A_{23}^{j,m} \\ 0 & A_{32}^{j,m} & 0 \end{bmatrix},\ B = \begin{bmatrix} 0 & B_{12}^{j,m} & 0 \\ 0 & B_{22}^{j,m} & 0 \\ B_{31}^{j,m} & 0 & B_{33}^{j,m} \end{bmatrix} \\ C &= \begin{bmatrix} C_{11}^{j,m} & 0 & C_{13}^{j,m} \\ 0 & 0 & C_{23}^{j,m} \\ 0 & C_{32}^{j,m} & 0 \end{bmatrix},\ p = \begin{bmatrix} p_m^1 \\ p_m^2 \\ p_m^3 \end{bmatrix}\end{aligned} \tag{21}$$

The elements expressions in matrix equations (21) are shown in Appendix 1.

Two new vector q is introduced, namely:

$$q = k\,p \tag{22}$$

Substituting Eq. (22) into Eq. (20):

$$k\ A\ q + \ B\ q + C\ p\ = 0 \tag{23}$$

According to Eqs. (22)-(23):

$$k\begin{bmatrix} p \\ q \end{bmatrix} = \begin{bmatrix} 0 & I \\ -A^{-1}C & -A^{-1}B \end{bmatrix}\begin{bmatrix} p \\ q \end{bmatrix} \tag{24}$$

where I is an identity matrix. The complex solution for k can be obtained by solving the eigenvalue problem presented by Eq. (24).

From the analysis of the matrix elements in Eq. (24), all integral types can be divided into the following three types:

$$G_i = \int_{-1}^{1} z^a P_j(z) \frac{d^{(i-1)}}{dz^{(i-1)}} P_m(z) dz \quad (i = 1,2,3) \tag{25}$$

Firstly, the expression of I_1 is deduced. The expression of $P_m(t)$ can be written (Wang *et al*. 2021, Yu *et al*. 2022)

$$P_m(t) = \sum_{v=0}^{\left\lfloor \frac{m}{2} \right\rfloor} (-1)^v \frac{(2m-2v)!}{2^m v!\,(m-v)!\,(m-2v)!} t^{m-2v} \tag{26}$$

Based on orthogonality and Eq. (26),

$$G_i = \begin{cases} \sum_{v=0}^{\left\lfloor \frac{m}{2} \right\rfloor} (-1)^v \frac{(2m-2v)!}{2^m v!\,(m-v)!\,(m-2v-i+1)!} \frac{2^{j+1}(j+2p)!\,(j+p)!}{p!\,(2j+2p+2-i)!}, & a+m-i+1 \geq j \text{ and } a+m-j-i+1 = \text{even} \\ 0, \quad \text{else} \end{cases} \tag{27}$$

where $a + m - i + 1 \geq j$ and $a + m - j - i + 1 =$ even.

$$\begin{cases} \int_0^h \left(\frac{2z-h}{h}\right)^a Q_j(z) Q_m(z) dz \\ = \frac{1}{2}\sqrt{(2j+1)(2m+1)} \int_{-1}^{1} z^a P_j(z) P_m(z) dz \\ \int_0^h \left(\frac{2z-h}{h}\right)^a Q_j(z) \frac{d}{dz} Q_m(z) dz \\ = \frac{1}{h}\sqrt{(2j+1)(2m+1)} \int_{-1}^{1} z^a P_j(z) \frac{d}{dz} P_m(z) dz \end{cases} \tag{28}$$

3.2 SH waves

According to Eq. (2), the SH wave governing equation is:

$$\frac{\partial \sigma_{xy}}{\partial x} + \frac{\partial \sigma_{zy}}{\partial z} = \rho(z) \frac{\partial^2 u_y}{\partial t^2} \tag{29}$$

According to Eqs. (4)-(6), the nonlocal constitutive relations of FGM plate can be expressed as:

$$\frac{\partial \sigma_{xy}}{\partial x} + \frac{\partial \sigma_{zy}}{\partial z} = \rho(z) \frac{\partial^2 u_y}{\partial t^2} \tag{30}$$

$$\sigma_{xy} - l^2\left(\frac{\partial^2 \sigma_{xy}}{\partial x^2} + \frac{\partial^2 \sigma_{xy}}{\partial z^2}\right) = \mu(z) \frac{\partial u_y}{\partial x} \tag{31}$$

Substituting Eq. (29) into Eqs. (30)-(31):

$$\mu(z) \frac{\partial}{\partial z}\left[\frac{1}{\rho(z)} \frac{\partial \sigma_{xy}}{\partial x} + \frac{1}{\rho(z)} \frac{\partial \sigma_{zy}}{\partial z}\right] - \frac{\partial^2}{\partial t^2}\left[\sigma_{zy} - l^2\left(\frac{\partial^2 \sigma_{zy}}{\partial x^2} + \frac{\partial^2 \sigma_{zy}}{\partial z^2}\right)\right] = 0 \tag{32}$$

$$\mu(z) \frac{\partial}{\partial x}\left[\frac{1}{\rho(z)} \frac{\partial \sigma_{xy}}{\partial x} + \frac{1}{\rho(z)} \frac{\partial \sigma_{zy}}{\partial z}\right] - \frac{\partial^2}{\partial t^2}\left[\sigma_{zy} - l^2\left(\frac{\partial^2 \sigma_{zy}}{\partial x^2} + \frac{\partial^2 \sigma_{zy}}{\partial z^2}\right)\right] = 0 \tag{33}$$

To satisfy the boundary conditions (σ_{zy} = 0, at z = 0 and z = h), the nonlocal stress of free harmonic waves are:

$$\sigma_{zy} = z(z-h)V(z)\, e^{i(kx-\omega t)} \tag{34}$$

$$\sigma_{xy} = W(z)\, e^{i(kx-\omega t)} \tag{35}$$

Then, V (z) and W (z) are expanded into Legendre orthogonal polynomial series:

$$V(z) = \sum_{m=0}^{\infty} p_m^1\, Q_m(z),\ W(z) = \sum_{m=0}^{\infty} p_m^2\, Q_m(z), \tag{36}$$

$$Q_m(z) = \sqrt{\frac{2m+1}{h}}\, L_m(\overline{z}) \tag{37}$$

Substituting Eqs. (34)-(37) into Eqs. (32) and (33), multiplying by $Q_j(z)$ (j = 0…M), and integrating on the interval [0, h], the following matrix equations can be obtained:

$$k^2 A\ p + k\ B\ p + C\ p\ = 0 \tag{38}$$

where

$$A = \begin{bmatrix} A_{11}^{j,m} & 0 \\ 0 & A_{22}^{j,m} \end{bmatrix}, B = \begin{bmatrix} 0 & B_{12}^{j,m} \\ B_{21}^{j,m} & 0 \end{bmatrix}, \quad C = \begin{bmatrix} C_{11}^{j,m} & 0 \\ 0 & C_{22}^{j,m} \end{bmatrix},\ p = \begin{bmatrix} p_m^1 \\ p_m^2 \end{bmatrix} \tag{39}$$

Then, the rest of the solution process is the same as the above Lamb wave case.

4. Results and discussion

4.1 Validation analyses

In order to verify the polynomial method, the FGM plate is considered as a limit case of layered structures (Golub *et al.*

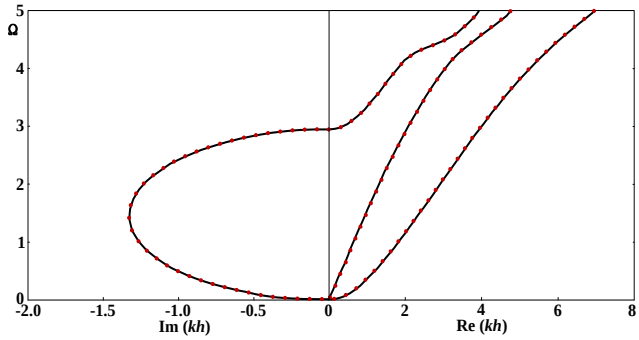

Fig. 2 Dispersion curves of Lamb waves in a nonlocal FGM plate; solid lines: the results obtained using AINSLPM; dot lines: the results obtained using the global matrix method

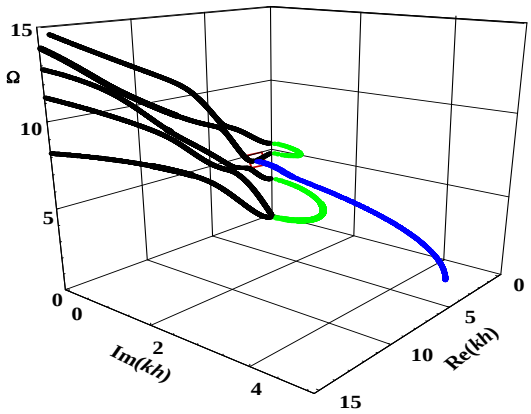

Fig. 3 Complete 3D dispersion curves of Lamb waves in nonlocal FGM plate

Table 1 The computational efficiency of AINSLPM and NSLPM (s)

M	6	8	10	12	14
NSLPM	10.125	40.766	208.87	583.95	1138.2
AINSLPM	0.766	0.860	0.937	1.063	1.157
Save (%)	92.435	97.890	99.551	99.818	99.898

2012), and the global matrix method is utilized to deduce the solutions. The solving process of the nonlocal multi-layer model by the global matrix method has been deduced in detail in the ref. (Yan *et al*. 2017). Materials 1 and 2 are selected as aluminum and silicon carbide, respectively. The material parameters of aluminum are E_1 = 70 GPa, ν_1 = 0.3, ρ_1 = 2702 kg/m^3, and the material parameters of silicon carbide are E_2 = 472 GPa, ν_2 = 0.17, ρ_2 = 3100 kg/m^3 (Ke and Wang, 2011). The thickness h is 4 nm. The volume distribution of FGM plate is assumed as the power function law of n = 1. The dimensionless angular frequency is defined as $\Omega = \omega h/\sqrt{(\mu_1+\mu_2)/(\rho_1+\rho_2)}$. Then, the dispersion curves of a nonlocal FGM plate obtained by both the AINSLPM and global matrix method (110 sub-layers) are compared, as shown in Fig. 2 It is clear that the two methods are in good agreement.

It is necessary to discuss the convergence and computational efficiency of the Legendre polynomial method. The convergence of the polynomial method is closely related to the Legendre series expansion order M. Especially when solving higher-order guided wave modes, the polynomial method needs to be expanded to a higher order. This leads to the NSLPM involving a large number of numerical integration steps, and computing these integrals is often computationally expensive. Table 1 shows the time taken to calculate a frequency point for NSLPM and AINSLPM under different Legendre series expansion order *M*. The parameters used in the example are $\Omega = 2$, l = 0.15 nm and n = 1. Different from NSLPM, AINSLPM uses analytical integration instead of numerical integration, and the computational efficiency is improved by more than 90%. The advantage of AINSLPM is more obvious, especially for high Legendre series expansion order.

4.2 Lamb wave

Firstly, the 3D dispersion curves of Lamb waves in nonlocal FGM plate are shown in Fig. 3 with nonlocal parameter l = 0.15 nm. The black lines are propagating Lamb waves with purely real wavenumber solutions. The green lines are exponentially decaying evanescent waves with purely imaginary wavenumber solutions. The blue lines are the evanescent waves with damped sinusoidal distribution decay, which correspond to the complex wavenumber solution. The first-order complex Lamb wave mode starts at zero frequency and intersects the propagating wave mode at the end point.

4.2.1 The intersection problem

Fig. 4 shows dispersion curves of propagating Lamb waves and complex evanescent waves (real part) in nonlocal aluminum plate, silicon carbide plate, mixed homogeneous plate and FGM plate, respectively. Here, the mixed homogeneous plate is made by mixing two materials uniformly with the same volume fraction, and its Lame constants are the average of the Lame constants of aluminum and silicon carbide. In addition, the mixed homogeneous model and linearly FGM model have the same material volume fraction. The black line, red line and blue line in Fig. 4 represent the anti-symmetric propagating Lamb waves, symmetric propagating Lamb waves and the real parts of complex evanescent waves, respectively. Different from homogeneous plates, due to the change of the FGM material properties, the Lamb waves (green line) of FGM plate in Fig. 4 (d) is not symmetric or anti-symmetric. It can be seen that the dispersion curves of anti-symmetric and symmetric propagating Lamb waves of the silicon carbide plate and mixed homogeneous plate in Figs. 4 (b) and (c) will have some intersections. However, there is no intersection between adjacent propagating modes of the aluminum plate and FGM plate in Figs. 4 (a) and (d).

In fact, the intersections between Lamb mode dispersion curves have practical significance in non-destructive evaluation and material characterization, for example, selection modes for studying nonlinearity by accumulating harmonic generation. It has shown that the intersections between anti-symmetric and symmetric propagating Lamb waves are conditioned by two additional real solutions of the Rayleigh cubic equation in the classical elastic theory,

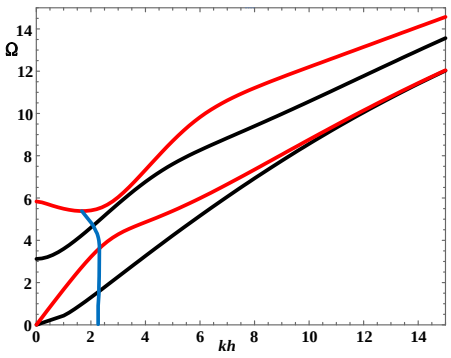

(a) nonlocal aluminum plate

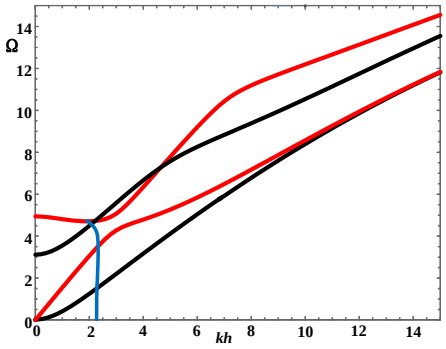

(b) nonlocal silicon carbide plate

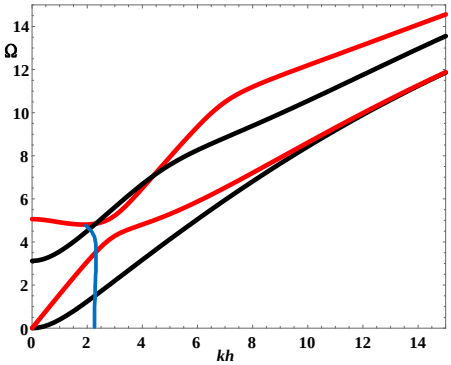

(c) nonlocal mixed homogeneous plate

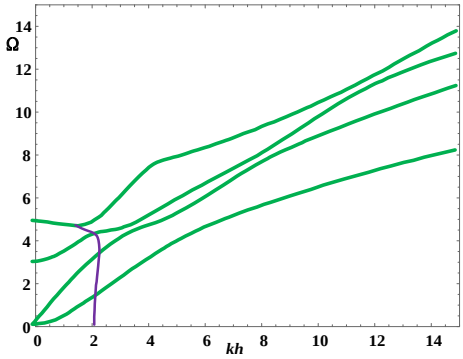

(d) nonlocal FGM plate

Fig. 4 Wave number dispersion curves of propagating and complex evanescent Lamb waves

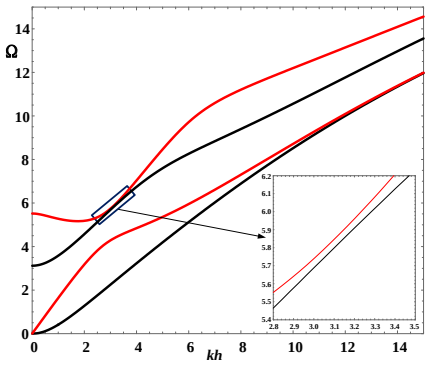

(a) v = 0.265

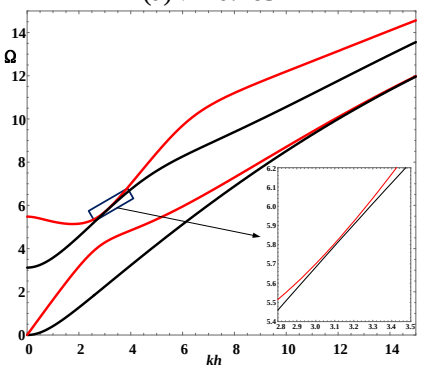

(b) v = 0.260

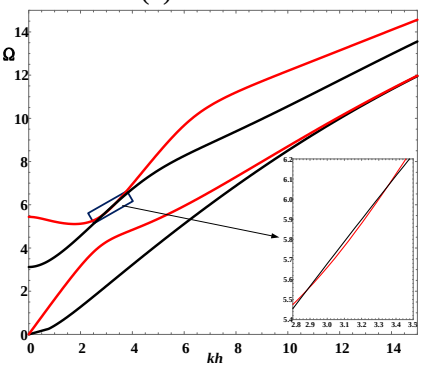

(c) v = 0.255

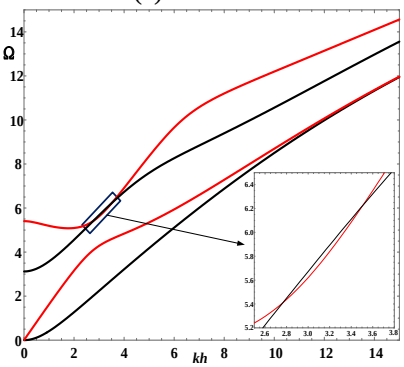

(d) v = 0.250

Fig. 5 Wave number dispersion curves of propagating Lamb wave and complex evanescent Lamb wave modes in nonlocal plate

and it appears at v <0.26308 (Every 2016). The Poisson's ratios of aluminum, silicon carbide and mixed homogeneous materials are v_1 = 0.3> 0.26308, v_2 = 0.17 <0.26308 and v_{mix} = 0.1934 <0.26308, respectively. To explore the restrictive conditions required for intersections in the context of the nonlocal theory, Fig. 5 presents the dispersion curves of four materials with different Poisson's ratios. The elastic modulus and density are E = 70 GPa and

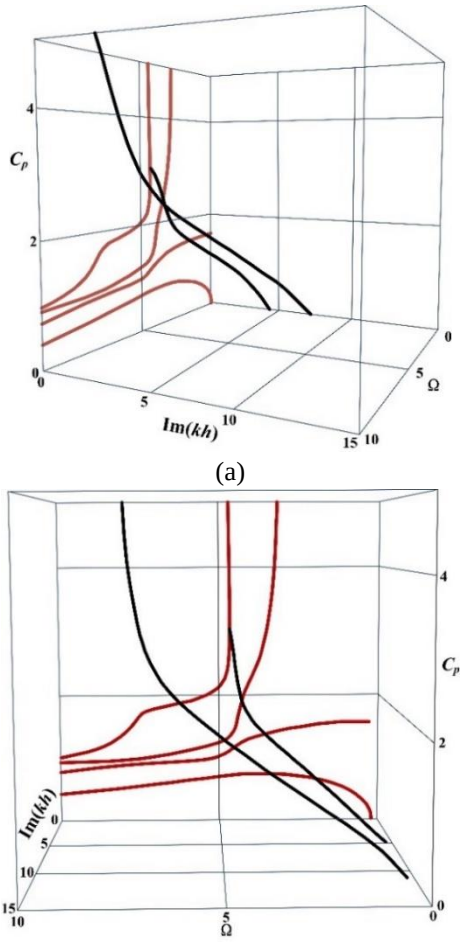

Fig. 6 3D Phase velocity dispersion curves of propagating and complex evanescent Lamb waves in nonlocal FGM plate; (a) and (b) show different viewing directions

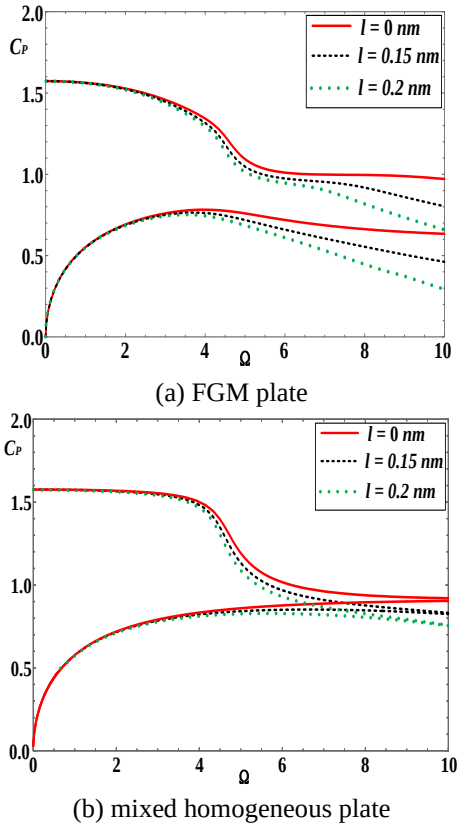

Fig. 7 Phase velocity dispersion curves of propagating Lamb waves

ρ = 2702 kg /m3. It can be observed that when the Poisson's ratio is v = 0.265 and 0.26, there is no intersection in the Lamb wave dispersion curve. However, when Poisson's ratio is v = 0.255 and 0.25, the adjacent symmetrical and antisymmetric Lamb wave modes cross each other. In other words, the intersections are still limited by the Poisson's ratio in the context of the nonlocal theory.

When the nonlocal parameter l = 0.15nm, the condition for the occurrence of intersections is ν <0.255 ~ 0.26. Compared with the classical elastic theory, the occurrence of intersections in the context of the nonlocal theory needs to meet the smaller Poisson's ratio condition. In fact, the Rayleigh equation of nonlocal theory has the same form as the corresponding equation of classical theory (Ac Harya and Mondal 2002). However, due to the correlation between nonlocal modulus and wavenumber and nonlocal parameters (Nowinski 1984), the conditions for the intersection between anti-symmetric and symmetrically propagating Lamb waves are more complicated. Due to its continuously changing material properties, the Lamb wave dispersion curves in the FGM plate change relatively smoothly. For this reason, even if the mixed homogeneous plate and FGM plate have the same material composition, the dispersion curves of adjacent propagating modes in FGM plate are close to each other but do not have intersections.

4.2.2 The inhomogeneity and nonlocal effects

Phase velocity dispersion curves of propagating and complex evanescent Lamb waves in nonloal FGM plate are shown in Fig. 6. The phase velocity and attenuation are represented by $C_p = \omega$ / Re (k) and Im (k), respectively. As shown in Fig. 6, complex evanescent Lamb waves have small attenuation and higher phase velocity than the propagating wave modes at some frequencies, which has great potential in structural health monitoring (Yan and Yuan 2018) and improving the energy conversion efficiency of devices.

First, the influences of nonlocal effects and inhomogeneity of medium on the phase velocity of the propagating Lamb waves are discussed. Figs. 7 (a) and (b) show the dispersion curves of propagating Lamb waves in FGM plate and mixed homogeneous plate with nonlocal parameters l = 0, 0.15 and 0.2 nm, respectively. The solutions for l = 0 correspond to the solutions of classical elastic theory. The size-dependent effect reduces the phase velocity of propagating Lamb waves due to the stiffness-softening effect predicted by the nonlocal theory. In the context of the classical elastic theory, the phase velocities of the first two propagating Lamb wave modes in the mixed homogeneous plate converge to the same Rayleigh wave velocity, while those in FGM plate converge to Rayleigh wave velocities of

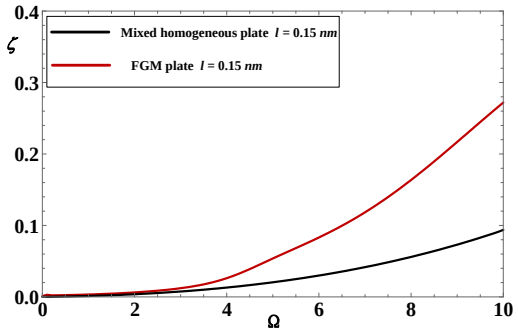

Fig 8 The nonlocal effect on phase velocity of propagating Lamb waves in FGM plate and mixed homogeneous plate

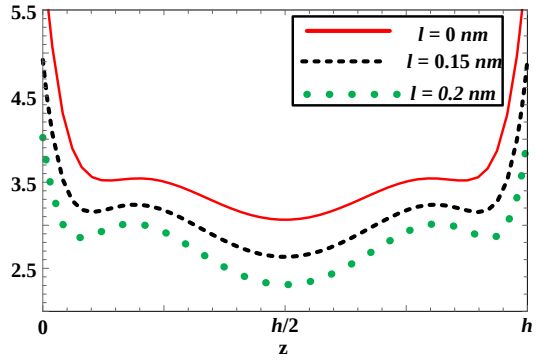

(a) in the directions x

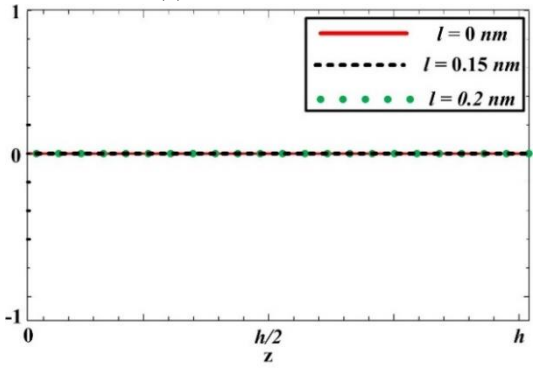

(b) in the directions z

Fig. 9 Poynting vector components of propagating Lamb waves in mixed homogeneous plate

materials 1 and 2, respectively. In nonlocal theory, the first two lamb wave phase velocities in the mixed homogeneous plate converge to the same velocity and decrease together, while those in FGM plate decrease at different phase velocities.

Here, a new variable $\zeta = |C_{p_{\text{nolocal}}} - C_{p_{\text{classical}}}|/C_{p_{\text{classical}}}$ is defined to describe the size-dependent effect, where $C_{p_{\text{nolocal}}}$ and $C_{p_{\text{classical}}}$ are phase velocities in nonlocal and classical elastic plate, respectively. The change of ζ with dimensionless frequency in FGM plate and mixed homogeneous plate are shown in Fig. 8. As the dimensionless frequency increases, the nonlocal parameters approach the wavelength, and the nonlocal effects become more obvious. The nonlocal effect in FGM structure is notably stronger

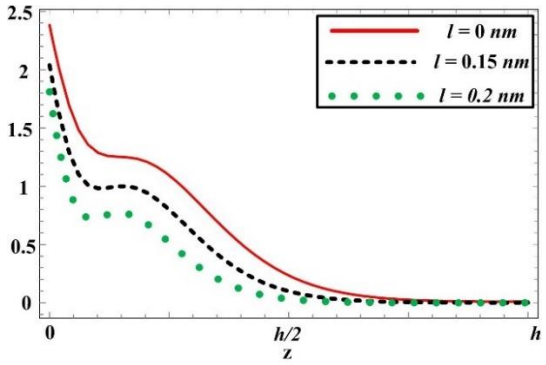

(a) in the directions x

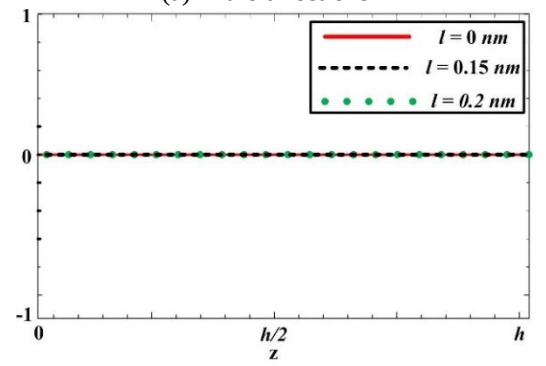

(b) in the directions z

Fig. 10 Poynting vector components of propagating Lamb waves in FGM plate

than the mixed homogeneous structure. The inhomogeneity of medium enhances the nonlocal effect on the phase velocity of propagating Lamb waves.

Then, the dimensionless Poynting vector components of the first propagating Lamb waves in mixed homogeneous plate at $\Omega = 6$ are shown in Fig. 9. The nonlocal parameters are l = 0, 0.15 and 0.2 nm (kh = 0.8757, 0.8499 and 0.8294), respectively. They are calculated by the following formula evaluated at x = 0 (Yu *et al*. 2017):

$$P_x = Re\left[\frac{i\omega}{2}(T_{xx}\ .\ u_x^* + T_{xz}\ .\ u_z^*)\right],$$
$$P_z = Re\left[\frac{i\omega}{2}(T_{xz}\ .\ u_x^* + T_{zz}\ .\ u_z^*)\right]. \quad (38)$$

Since the energy of the wave propagates in the x direction, the Poynting vector in the z direction is zero, but the Poynting vector in the x direction is not zero. It can be seen from Fig. 9 that the nonlocal effect reduces the Poynting vector distribution. Fig. 10 shows the dimensionless Poynting vector components of the first propagating Lamb wave mode in FGM plate. Different from the homogeneous plate, the Poynting vector distribution is asymmetric with respect to the thickness direction and is mainly distributed near the side with low wave velocity.

Fig. 11 shows phase velocity dispersion curves of complex evanescent Lamb waves. It is observed that the nonlocal effect make complex evanescent Lamb waves have higher phase velocities at low attenuation. The complex Lamb waves can only propagate within a limited

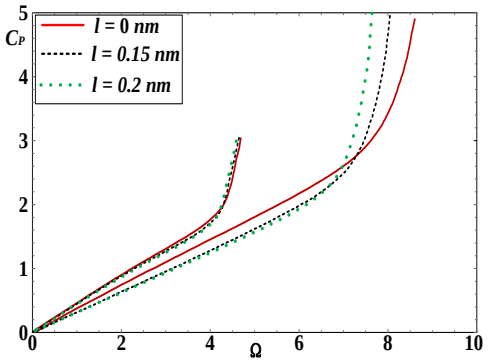

(a)

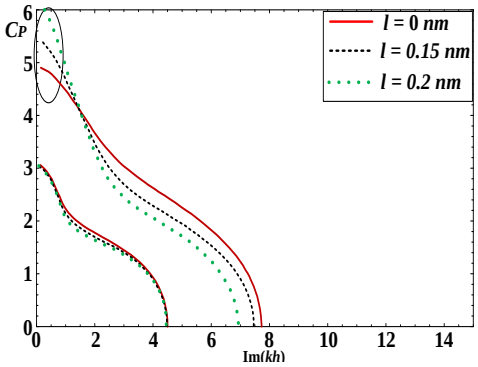

(b)

Fig. 11 Phase velocity dispersion curves of complex evanescent Lamb waves in FGM plate with different l

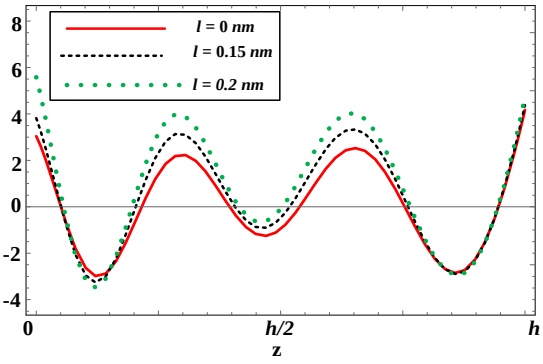

(a) in the directions *x*

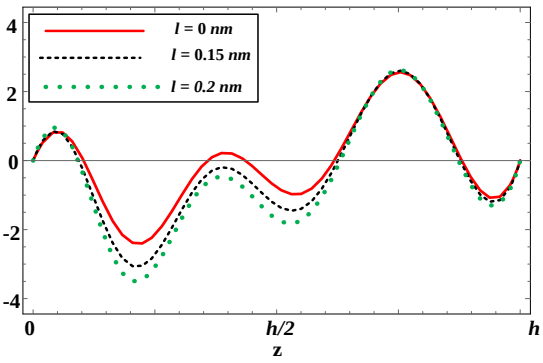

(b) in the directions *z*

Fig. 13 Poynting vector components of the complex evanescent Lamb waves in FGM plate

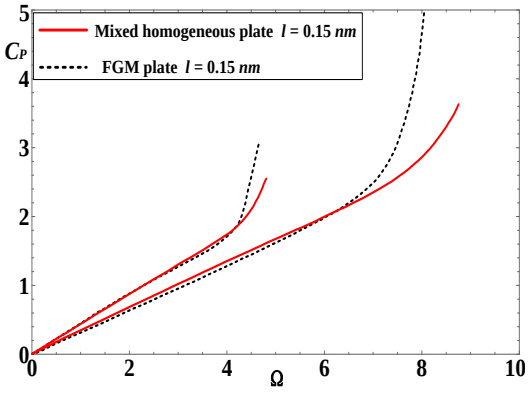

(a)

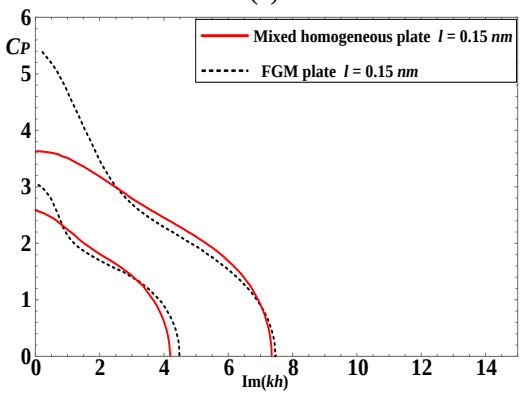

(b)

Fig. 12 Phase velocity dispersion curves of complex evanescent Lamb waves in FGM plate and mixed homogeneous plate

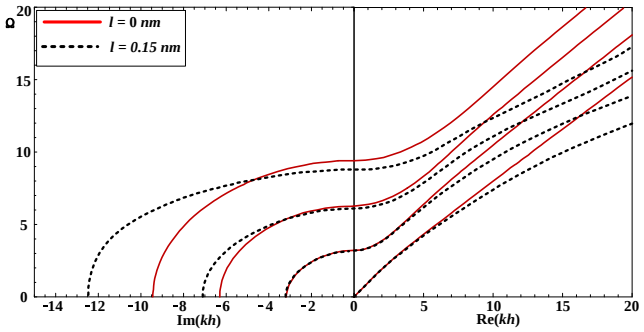

Fig. 14 Wave number dispersion curves of propagating SH wave and evanescent SH wave modes in FGM plate

bandwidth. For an example, when Ω > 4.8, the first complex Lamb wave mode will not exist.

Fig. 12 shows dispersion curves of complex evanescent Lamb in FGM plate and mixed homogeneous plate. The inhomogeneity of medium reduces the frequency bandwidth of the complex evanescent Lamb waves, and makes the complex evanescent Lamb waves have a higher phase velocity at low attenuation.

The Poynting vector components of the complex evanescent Lamb waves in FGM plate at $\Omega = 6$ are presented in Fig. 13. The nonlocal parameters are l = 0, 0.15 and 0.2 nm (kh = 2.7967+5.1838i, 2.8560+4.9908i and 2.8735+4.8447i), respectively. The Poynting vectors in the z and x directions are not zero due to the local vibration and local propagation. Different from the case of the propagating mode Poynting, the nonlocal effect enhances the Poynting

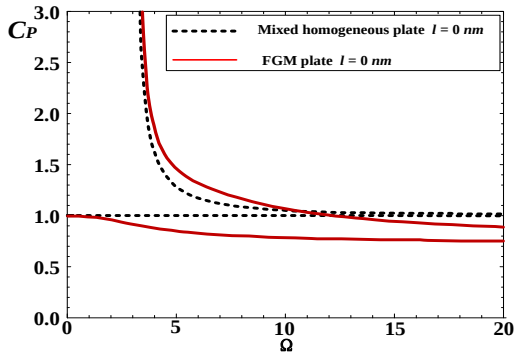

(a)

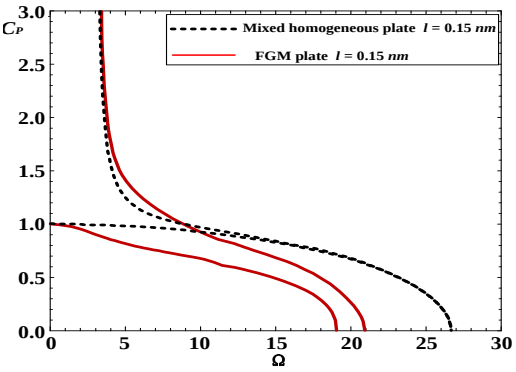

(b)

Fig. 15 Phase velocity dispersion curves of propagating SH waves in FGM plate and mixed homogeneous plate

distribution of the complex evanescent Lamb waves. The effect of nonlocality on the attenuation of complex evanescent waves can be used to explain their effect on the Poynting vector. Fig. 11 has shown that the nonlocal effect reduces the attenuation of complex evanescent waves at the corresponding frequencies. That is, the nonlocal effect enables the complex evanescent wave to travel farther in the propagation direction. From this point of view, the nonlocal effect enhances the energy of the complex evanescent waves, that is, increases its Poynting vector.

4.3 SH wave

Fig. 14 shows the SH wavenumber dispersion curve with l = 0 and 0.15 nm in the FGM plate. Materials 1 and 2 are stainless steel and silicon nitride, whose material constants are ρ_1 = 8166 kg/m^3, λ_1 = 136.67 GPa, μ_1 = 78.899 GPa and ρ_2 = 2370 kg/m^3, λ_2 = 120 GPa, μ_2 = 130 GPa (Zhang *et al*. 2019). Unlike Lamb waves, there are only propagating SH waves and purely imaginary evanescent SH waves, and no complex evanescent SH waves.

5. Conclusions

The analytical integration nonlocal stress expansion Legendre polynomial method is developed to study the propagating and evanescent waves. The complex guided waves in FGM nanoplate are solved. The nonlocal effects, inhomogeneity of medium and their interactions on wave dynamic analysis are presented. Some main conclusions can be drawn:

• In the nonlocal homogeneous plate, the occurrence of intersections of propagating Lamb wave modes is still limited by the Poisson's ratio, and it needs to satisfy a smaller Poisson's ratio condition than that in the classical elastic theory.

• In the FGM plate, the occurrence of mode intersections needs to meet a much smaller Poisson's ratio condition than that in the homogeneous plate.

• The inhomogeneity of medium enhances the nonlocal effect on the phase velocity.

• The nonlocal effects and inhomogeneity reduce the frequency bandwidth of complex evanescent Lamb waves, and make complex evanescent Lamb waves have a higher phase velocity at low attenuation.

• Different propagating SH wave modes in the nonlocal homogeneous plate have the same escape frequency, while those in the FGM plate have different escape frequencies.

• The nonlocal effect reduces the Poynting vectors of the propagating Lamb waves and increases the Poynting vectors of the complex evanescent Lamb waves.

The conclusions obtained can be applied to the design and dynamic response evaluation of composite nano-structures. For example, adjustment of size-dependent features using functionally graded material properties, inversion of material size parameters using energy distribution, and mode selection for studying non-linearity through cumulative harmonic generation, etc.

Acknowledgments

The authors gratefully acknowledge the support by the National Natural Science Foundation of China (No. 51975189 and No.12102131), the Project funded by China Postdoctoral Science Foundation under grant numbers 2021M701102.

References

Ac Harya, D.P. and Mondal, A. (2002), "Propagation of Rayleigh surface waves with small wavelengths in nonlocal visco-elastic solids", *Sadhana*, **27**(6), 605-612. https://doi.org/10.1007/BF02703353.

Ahmadi, I. (2021), "Vibration analysis of 2d-functionally graded nanobeams using the nonlocal theory and meshless method", *Eng. Anal. Bound. Elem*., **124**(8), 142-154. https://doi.org/10.1016/j.enganabound.2020.12.010.

Amiri, A., Vesal, R., and Talebitooti, R. (2019), "Flexoelectric and surface effects on size-dependent flow-induced vibration and instability analysis of fluid-conveying nanotubes based on flexoelectricity beam model", *Int. J. Mech. Sci.*, **156**, 474-485. https://doi.org/10.1016/j.ijmecsci.2019.04.018.

Arefi, M. (2016). "Surface effect and non-local elasticity in wave propagation of functionally graded piezoelectric nano-rod excited to applied voltage", *Appl. Math. Mech-Engl*., **37**(3), 289-302. https://doi.org/10.1007/s10483-016-2039-6.

Asghari Ardalani, A.R., Amiri, A., Talebitooti, R., and Safizadeh, M.S. (2021), "On wave dispersion characteristics of fluid-conveying smart nanotubes considering surface elasticity and flexoelectricity approach", *P. I. Mech. Eng. C. J. Mec*., **235**(18),

3506-3518. https://doi.org/10.1177/0954406220965611.

Cao, X., Jiang, H., Ru, Y., and Shi, J. (2019), "Asymptotic solution and numerical simulation of lamb waves in functionally graded viscoelastic film", *Materials*, **12**(2), 1-16. https://doi.org/10.3390/ma12020268

Chaht, F. L., Kaci, A., Houari, M., Tounsi, A. and Mahmoud, S. R. (2015), "Bending and buckling analyses of functionally graded material (FGM) size-dependent nanoscale beams including the thickness stretching effect", *Steel Compos. Struct.*, **18**(2), 425-442. https://doi.org/10.12989/scs.2015.18.2.425

Cha, S.N., Seo, J.S., Kim, S.M., Kim, H.J., Park, Y.J., Kim, S.W. and Kim, J.M. (2010), "Sound-driven piezoelectric nanowire-based nanogenerators", *Adv. Mater.*, **22**(42), 4726-4730. https://doi.org/10.1002/adma.201001169.

Chong, K.P (2008), "Nano science and engineering in solid mechanics", *Acta Mech. Solida Sin.*, **21**(002), 95-103. https://doi.org/10.1007/s10338-008-0812-7

Ebrahimi, F., Barati, M.R., Dabbagh, A. (2018a), "Wave propagation in embedded inhomogeneous nanoscale plates incorporating thermal effects", *Wave Random Complex*, **28**(2), 215-235. https://doi.org/10.1080/17455030.2017.1337281

Ebrahimi, F. and Haghi, P. (2018b), "Elastic wave dispersion modelling within rotating functionally graded nanobeams in thermal environment", *Adv. Nano Res., Int. J.*, **6**(3), 201-217. https://doi.org/10.12989/anr.2018.6.3.201

Ehyaei, J., Ebrahimi, F. and Salari, E. (2016), "Nonlocal vibration analysis of FG nano beams with different boundary conditions", *Adv. Nano Res.*, **4**(2), 85-111. https://doi.org/10.12989/anr.2016.4.2.085

Elayan, H., Shubair, R.M., Jornet, J.M. and Mittra, R. (2017), "Multi-layer intrabody terahertz wave propagation model for nanobiosensing applications", *Nano Commun. Netw.*, **14**(DEC.), 9-15. https://doi.org/10.1016/j.nancom.2017.08.005

Eringen, A.C. (1983), "On differential equations of nonlocal elasticity and solutions of screw dislocation and surface waves", *J. Appl. Phys.*, **54**(9), 4703-4710. https://doi.org/10.1063/1.332803.

Every, A.G. (2016), "Intersections of the Lamb mode dispersion curves of free isotropic plates", *J. Acoust. Soc. Am.*, **139**(4), 1793. http://doi.org/10.1121/1.4946771

Ghayesh, M.H. and Farajpour, A. (2019), "A review on the mechanics of functionally graded nanoscale and microscale structures", *Int. J. Eng. Sci.*, **137**, 8-36. https://doi.org/10.1016/j.ijengsci.2018.12.001

Golub, M.V., Fomenko, S.I., Bui, T.Q., Zhang, C. and Wang, Y.S. (2012), "Transmission and band gaps of elastic SH waves in functionally graded periodic laminates", *Int. J. Solids Struct.*, **49**(2), 344-354. https://doi.org/10.1016/j.ijsolstr.2011.10.013

Gopalakrishnan S and Narendar S. (2013), *Wave Propagation in Nanostructures: Nonlocal Continuum Mechanics Formulations*, Springer Science & Business Media, New York, U.S.A.

Hadji, L. and Avcar, M. (2021), "Nonlocal free vibration analysis of porous FG nanobeams using hyperbolic shear deformation beam theory", *Adv. Nano Res., Int. J.*, **10**(3), 281-293. https://doi.org/10.12989/anr.2021.10.3.281

He, D., Shi, D., Wang, Q. and Ma, C. (2021), "Free vibration characteristics and wave propagation analysis in nonlocal functionally graded cylindrical nanoshell using wave-based method", *J. Brazil Soc. Mech. Sci. Eng.*, **43**(6), 292. https://doi.org/10.1007/s40430-021-03008-2

Hernandez, C.M., Murray, T.W. and Krishnaswamy, S. (2002), "Photoacoustic characterization of the mechanical properties of thin films", *Appl. Phys. Lett.*, **80**(4), 691-693. https://doi.org/10.1063/1.1434303

Jornet J M and Akyildiz I F. (2013), "Graphene-based plasmonic nano-antenna for terahertz band communication in nano-networks", *IEEE J. Sel. Area. Comm.*, **31**(12), 685-694. https://doi.org/10.1109/JSAC.2013.SUP2.1213001

Kaviani, F. and Mirdamadi, H.R. (2013), "Wave propagation analysis of carbon nano-tube conveying fluid including slip boundary condition and strain/inertial gradient theory", *Comput. Struct.*, **116**, 75-87. https://doi.org/10.1016/j.compstruc.2012.10.025

Ke, L.L. and Wang, Y.S. (2011), "Size effect on dynamic stability of functionally graded microbeams based on a modified couple stress theory", *Compos. Struct.*, **93**(2), 342-350. https://doi.org/10.1016/j.compstruct.2010.09.008

Kuznetsov S.V. (2019), "Cauchy formalism for Lamb waves in functionally graded plates", *J. Vibr. Control.*, **25**(6), 1227-1232. https://doi.org/10.1177/1077546318815376

Kuznetsov, S.V. (2021), "Lamb waves in stratified and functionally graded plates: Discrepancy, similarity, and convergence", *Wave Random Complex*, **31**(6), 1540-1549. https://doi.org/10.1080/17455030.2019.1683257

Liu, C.C., Yu, J.G., Xu, W.J., Zhang, X.M. and Wang, X.H. (2021), "Dispersion characteristics of guided waves in functionally graded anisotropic micro/nano-plates based on the modified couple stress theory", *Thin Wall Struct.*, **161**, 107527. https://doi.org/10.1016/j.tws.2021.107527

Liu, C.C., Yu, J.G., Zhang, B., Wang, X.H., Zhang, X.M., and Zhang, H.D. (2022), "Complete guided wave in piezoelectric nanoplates: A nonlocal stress expansion polynomial method", *Eur. J. Mech. A Solids*, **94**, 104588. https://doi.org/10.1016/j.euromechsol.2022.104588

Lu, P., He, L.H., Lee, H.P. and Lu, C. (2006), "Thin plate theory including surface effects", *Int. J. Solids Struct.*, **43**(16), 4631-4647. https://doi.org/10.1016/j.ijsolstr.2005.07.036

Luat, D.T., Thom, D.V., Thanh, T.T., Phung, M. and Vinh, P.V. (2021), "Mechanical analysis of bi-functionally graded sandwich nanobeams", *Adv. Nano Res.*, **11**(1), 55-71. https://doi.org/10.12989/anr.2021.11.1.055

Lyon, R.H. (1955), "Response of an elastic plate to localized driving forces", *J. Acoust. Soc. Am.*, **27**, 259-265. https://doi.org/10.1121/1.1907510

Mindlin, R.D. (1965), "Second gradient of strain and surface-tension in linear elasticity", *Int. J. Solids Struct.*, **1**(4), 417-438. https://doi.org/10.1016/0020-7683(65)90006-5

Mindlin, R.D. (1958), "Vibrations of an infinite elastic plate at its cutoff frequencies", *Proceedings of the Third U.S. National Congress of Applied Mechanics*, 225-226.

Mindlin, R.D., Medick, M.A. (1959), "Extensional vibrations of elastic plates", *J. Appl. Mech.*, **26**(4), 561-569. https://doi.org/10.1115/1.4012112

Nejad, M.Z., Hadi, A. and Rastgoo, A. (2016), "Buckling analysis of arbitrary two-directional functionally graded Euler-Bernoulli nano-beams based on nonlocal elasticity theory", *Int. J. Eng. Sci.*, **103**, 1-10. https://doi.org/10.1016/j.ijengsci.2016.03.001

Nowinski, J.L. (1984), "On the nonlocal theory of wave propagation in elastic plates", *J. Appl. Mech.*, **51**(3), 608-613. https://doi.org/10.1115/1.3167681

Othmani, C., Zhang, H. and Lu, C.F. (2020), "Effects of initial stresses on guided wave propagation in multilayered PZT-4/PZT-5A composites: A polynomial expansion approach", *Appl. Math. Model.*, **78**, 148-168. https://doi.org/10.1016/j.apm.2019.10.017

Oveissi, S. and Ghassemi, A. (2018), "Longitudinal and transverse wave propagation analysis of stationary and axially moving carbon nanotubes conveying nano-fluid", *Appl. Math. Model.*, **60**, 460-477. https://doi.org/10.1016/j.apm.2018.03.004

Quintanilla, F.H., Lowe, M.J.S. and Craster, R.V., (2016), "Full 3D dispersion curve solutions for guided waves in generally anisotropic media", *J. Sound. Vib.*, **363**, 545-559. https://doi.org/10.1016/j.jsv.2015.10.017

Tran, T.T., Tran, V.K., Pham, Q.H. and Zenkour, A.M. (2021),

"Extended four-unknown higher-order shear deformation nonlocal theory for bending, buckling and free vibration of functionally graded porous nanoshell resting on elastic foundation", *Compos. Struct*., **264**(1), 113737. https://doi.org/10.1016/j.compstruct.2021.113737

Wang, X., Li, F., Zhang, X., Yu, J., and Qiao, H. (2021), "Thermoelastic guided wave in fractional order functionally graded plates: An analytical integration Legendre polynomial approach", *Compos. Struct*., **256**, 112997. https://doi.org/10.1016/j.compstruct.2020.112997.

Yan, D.J., Chen, A.L., Wang, Y.S., Zhang, C.Z. and Golub, M. (2017), "Propagation of guided elastic waves in nanoscale layered periodic piezoelectric composites", *Eur. J. Mech. A-Solid*, **66**, 158-167. https://doi.org/10.1016/j.euromechsol.2017.07.003

Yan, X. and Yuan, F.G. (2015), "Conversion of evanescent Lamb waves into propagating waves via a narrow aperture edge", *J. Acoust. Soc. Am*., **137**(6), 3523-3533. https://doi.org/10.1121/1.4921599

Yan, X., and Yuan, F.G., (2018), "A semi-analytical approach for SH guided wave mode conversion from evanescent into propagating", *Ultrasonics*, **84**, 430-437. https://doi.org/10.1016/j.ultras.2017.12.006

Yang, C., Yu, J., Liu, C., Zhang, B. (2022), "Elastic wave reflection/transmission in non-homogeneous magneto-electro-elastic nanoplates based on the modified couple stress theory", *Mech Solids+*, https://doi.org/10.3103/S0025654422020121

Yang, F., Chong, A., Lam, D. and Tong, P. (2002), "Couple stress based strain gradient theory for elasticity", *Int. J. Solids Struct*., **39**(10), 2731-2743. https://doi.org/10.1016/S0020-7683(02)00152-X

Yu, J.G., Lefebvre, J.E., Xu, W.J., Benmeddour, F. and Zhang, X.M. (2017), "Propagating and non-propagating waves in infinite plates and rectangular cross section plates: orthogonal polynomial approach", *Acta. Mech.*, **228** (11), 1-15. https://doi.org/10.1007/s00707-017-1917-1

Yu, J., Wang, X., Zhang, X., Li, Z., Li, F. (2022), "An analytical integration Legendre polynomial series approach for Lamb waves in fractional order thermoelastic multilayered plates", *Math. Method. Appl. Sci*., **45**(12), 7631-7651. https://doi.org/10.1002/mma.8266

Zhang, B., Yu, J.G., Lefebvre, J.E., Xu, W.J., Zhang, X.M. and Ming, P.M. (2019), "Guided wave propagation in functionally graded cylindrical structures with sector cross-sections", *Math. Mech. Solids*, **24**(2), 434-447. https://doi.org/10.1177/1081286517742433

Zhang, B., Wang, X.H., Elmaimouni, L., Yu, J.G. and Zhang, X.M. (2022), "Axial guided wave characteristics in functionally graded one-dimensional hexagonal piezoelectric quasi-crystal cylinders", *Math. Mech. Solids*, **27**(1), 125-143. https://doi.org/10.1177/10812865211013458

Zhang, K., Ge, M.H., Zhao, C., Deng, Z.C. and Xu, X.J. (2019), "Free vibration of nonlocal Timoshenko beams made of functionally graded materials by Symplectic method", *Compos. Part B Eng.*, **156**, 174-184. https://doi.org/10.1016/j.compositesb.2018.08.051

Zhang X, Li Z, Yu J. (2018), "The Computation of complex dispersion and properties of evanescent Lamb wave in functionally graded piezoelectric-piezomagnetic plates", *Materials*, **11**(7), 1186. https://doi.org/10.3390/ma11071186

Zhang, Y.W., Chen, J., Zeng, W., Teng, Y.Y., Fang, B. and Zang, J. (2015), "Surface and thermal effects of the flexural wave propagation of piezoelectric functionally graded nanobeam using nonlocal elasticity", *Comp. Mater. Sci.*, **97**, 222-226. https://doi.org/10.1016/j.commatsci.2014.10.046.

Zhu, F., Wang, B., Qian, Z.H. and Pan, E.N. (2018), "Accurate characterization of 3D dispersion curves and mode shapes of waves propagating in generally anisotropic viscoelastic/elastic plates", *Int. J. Solids Struct*., **150**, 52-65. https://doi.org/10.1016/j.ijsolstr.2018.06.001.

SR

Appendix: The elements in matrix equations (21)

$$A_{11}^{j,m}=\int_0^{\hbar} Q_j(z)Q_m(z)\rho(z)[-\lambda(z)-2\mu(z)+l^2\omega^2\rho(z)]\,dz \tag{A1}$$

$$A_{21}^{j,m}=\int_0^{\hbar} -Q_j(z)Q_m(z)\rho(z)\lambda(z)\,dz \tag{A2}$$

$$A_{23}^{j,m}=\int_0^{\hbar} -Q_j(z)Q_m(z)\rho^2(z)l^2\omega^2(\hbar-z)z dz \tag{A3}$$

$$A_{32}^{j,m}=\int_0^{\hbar} Q_j(z)Q_m(z)\rho(z)[\mu(z)-l^2\omega^2\rho(z)](\hbar-z)z dz \tag{A4}$$

$$\begin{aligned}B_{12}^{j,m}=\int_0^{\hbar} -iQ_j(z)\{&[\lambda(z)+2\mu(z)]\rho(z)[(\hbar-2z)\\&Q_m(z)+(\hbar-z)z\,Q_m'(z)]+\lambda(z)(\hbar-z)z\rho(z)\\&Q_m'(z)+\lambda(z)Q_m(z)[\rho(z)z(z-\hbar)]'(z)]\}dz\end{aligned} \tag{A5}$$

$$\begin{aligned}B_{22}^{j,m}=\int_0^{\hbar} -iQ_j(z)\{&\lambda(z)\rho(z)[(\hbar-2z)Q_m(z)\\&+(\hbar-z)z\,Q_m'(z)]+[\lambda(z)+2\mu(z)](\hbar-z)z\rho(z)Q_m'(z)\\&+[\lambda(z)+2\mu(z)]Q_m(z)[\rho(z)z(z-\hbar)]'(z)]\}dz\end{aligned} \tag{A6}$$

$$B_{31}^{j,m}=\int_0^{\hbar} i\mu(z)Q_j(z)[\rho(z)Q_m(z)]'(z)dz \tag{A7}$$

$$B_{33}^{j,m}=\int_0^{\hbar} -i\mu(z)Q_j(z)\rho(z)[Q_m(z)z(\hbar-z)]'(z)dz \tag{A8}$$

$$C_{11}^{j,m}=\int_0^{\hbar} Q_j(z)\omega^2\rho^2(z)[Q_m(z)-l^2Q_m''(z)]dz \tag{A9}$$

$$\begin{aligned}C_{13}^{j,m}=\int_0^{\hbar} Q_j(z)\lambda(z)\{&(\hbar-z)z\rho'(z)Q_m'(z)\\&+[2\rho(z)+(\hbar-2z)\rho'(z)]Q_m(z)\\&+\rho(z)[-2(\hbar-2z)Q_m'(z)+z(z-\hbar)Q_m''(z)]\}dz\end{aligned} \tag{A10}$$